An experimental study of the effects of plagioclase crystallization on REE behavior and Eu valence oxybarometry in pyroxene. P.V. Burger[1], C.K. Shearer[1], J.J. Papike[1], L. Le [2], J. Jones [2], S.R. Sutton[3,4] and M. Newville[4]. [1]Institute of Meteoritics, Department of Earth and Planetary Sciences, University of New Mexico, Albuquerque, NM, 87131 (pvburger@unm.edu), [2] Johnson Space Center, Houston, TX, 77058, [3]Department of Geophysical Sciences, University of Chicago, Chicago, IL, 60637, [4]Center for Advanced Radiation Sources, University of Chicago, Chicago, IL, 60637.

Introduction The effect of f_{O2} on the relative proportions of divalent and trivalent Eu is a useful tool for estimating f_{O2} in a variety of magmatic systems [1]. The concept of using Eu valence as a quantitative oxybarometer was initially demonstrated by [2,3]. The variation of $D_{Eu}^{plagioclase-melt}$ with oxygen fugacity has been determined experimentally by several workers and used to infer the redox conditions under which magmas have crystallized [4]. The behavior of Eu in pyroxene from martian basalts has proven to be an effective measure of f_{O2} [5]. These studies have demonstrated the power of Eu valence as an oxybarometer, and have hinted at numerous variables that influence the behavior of REE and Eu in pyroxene (e.g. melt chemistry, f_{O2}). The importance of many of these variables on major and minor elements in lunar pyroxenes was demonstrated by [6]. Detailed crystal-chemical rationale for REE and Eu behavior in pyroxenes from lunar basalts were explored by [7] and in angrites by [8]. In this study, we have synthesized a series of experiments based on the bulk chemistry of martian basalt QUE 94201 [9]. These experiments crystallized under a range of different conditions of f_{O2}, from IW-1 through QFM, at temperatures ranging from 950-1300 C. Initially, those samples without plagioclase on the liquidus were examined to determine $D_{Eu2+}^{pyroxene-melt}$ and $D_{Eu3+}^{pyroxene-melt}$ by [9]. This study expands on those results by characterizing the effect of plagioclase crystallization on pyroxene REE chemistry and the interpretation of the pyroxene oxybarometer.

Analytical Methods Samples were first categorized using a combination of electron microprobe (EPMA) backscattered electron imaging (BSE), quantitative analysis and wavelength dispersive (WDS) mapping. Select samples (QUE 24) have been further investigated for REE systematics by secondary ion mass spectrometry (SIMS) and x-ray, near edge structure (XANES) spectroscopy to determine the valence state of Eu (QUE 23 and 24, at f_{O2} of IW and IW+1, respectively). The samples used in this study were synthesized from a martian basalt (QUE 94201) composition [9] doped with several REEs, V, and Sc. The REEs were added as 0.6 wt% of each of their oxides, (i.e., REE_2O_3) and included La, Ce, Nd, Sm, Eu, Dy, Er, Yb and Lu. Scandium and vanadium were added as Sc_2O_3 and V_2O_3 and doped to 0.1 wt%. Experiments were conducted at several f_{O2} ranging from IW-1 to QFM. Additional information on the methodology used in preparing these samples can be found in [9]. Pyroxene, plagioclase, and glass were analyzed using a JEOL JXA 8200 EPMA at 15 kV, 20 nA, and a 1 µm beam, for major and minor elements. Trace element concentrations were determined using a Cameca IMS 4f ion probe with an accelerating voltage of 10 kV and primary beam

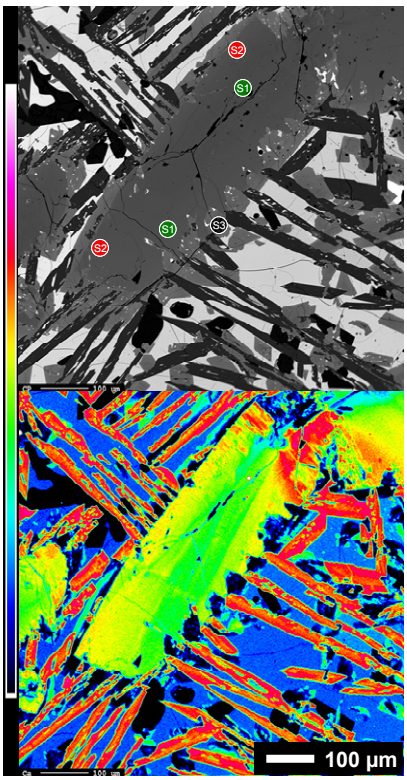

Figure 1. One of several pyroxene grains in QUE 24 (IW+1), analyzed in this study. a. BSE image. Colored dots represent the SIMS analytical spots seen in Fig. 3. Green indicates early, Mg-rich pyroxene, red dots represent augite, prior to plagioclase crystallization, and black spots represent late-stage (post plagioclase) crystallization. b. Calcium WDS map of analysis area.

current of 10 nA, which produced a spot size of ~20 µm. The ion probe analyses involved repeated cycles of peak counting on the isotopes ^{45}Sc, ^{51}V, ^{52}Cr, ^{139}La, ^{140}Ce, ^{146}Nd, ^{147}Sm, ^{151}Eu, ^{153}Eu, ^{163}Dy, ^{166}Er, and ^{174}Yb. Absolute concentrations of the trace elements were calculated using the relationship between measured peak/^{30}Si ratio, normalized to known SiO_2 content and elemental abundance in the standards. XANES analyses were performed with the GeoSoilEnviroCARS X-ray microprobe at the Advanced Photon Source (APS), Argonne National Laboratory, Illinois, using techniques described by [10]. The microprobe consisted of an APS undulator X-ray source, a silicon (111) double-crystal monochromator, Kirkpatrick-Baez microfocusing mirrors and an Oxford Instruments WDX-600 WDS detector with LiF200 crystal, using both sealed and flow proportional counters in tandem. The X-ray microprobe was used to determine average Eu valence in pyroxene, plagioclase and glass with a ~2 µm spatial resolution. The proportions of the two species were determined from the relative intensities of these peaks after calibration with the end-member standards, $Eu^{2+}TiO_3$ and $Eu^{3+}{}_2O_3$, which were measured as powders in transmission mode [9]. The estimated precision of the Eu valence determinations is ~0.03 (1σ).

Results Pyroxene crystallization begins with the nucleation of the most Mg-rich pigeonite (Fig. 1,2). Initial pyroxene crystallization is characterized by an increase of Ca activity in the melt, as plagioclase crystallization is delayed. With increased crystallization, pyroxene grains becomes more augitic, resulting in the increased compliancy of the M2 (6-8 fold coordinated) crystallographic site. This increased compliancy, coupled with the increasing concentration of REE^{3+} in the melt, results in greater degrees of REE partitioning into pyroxene. Furthermore, the M2 site becomes increasingly receptive to Eu^{2+} in the M2 site. With the onset of plagioclase crystallization, pyroxenes become more Fe-rich as the melt becomes depleted in Al, and to a lesser extent, Ca. At this stage, the M2 site should begin to contract, resulting in a decrease of REE^{3+} in still crystalizing pyroxene. Aluminum and Ti, which up to this point had both been steadily increasing in the melt, become decoupled (Fig. 2); later stage pyroxene crystallization is characterized by a rapid decrease in Al, as well as the continued incorporation of Ti at steady or ever increasing concentrations. Fortuitously, plagioclase grains in the QUE 24 (IW+1) and QUE 23 (IW) experiments nucleated onto existing pyroxene grains, providing a petrologic snapshot of the crystallization process (Fig.1). Wavelength dispersive mapping (WDS) for Ca in pyroxene grains provides a means of identifying potential analytical points for SIMS analyses of trace and REE, as well as ideal locations for XANES analyses of Eu valence (Fig.1). SIMS analyses were conducted comparing early stage, Mg-rich pigeonite, followed by more augitic pyroxene, and finally more Fe-rich, late stage pigeonite which crystallized concurrently with plagioclase. REE patterns (Fig.3) suggest that early stages of pyroxene crystallization are characterized by a LREE-depleted pattern with a moderate, negative Eu anomaly. Increased compliancy in the M2 site with increases in Ca lead to an overall increase in REE concentration, as the larger ionic-radius, trivalent REE are more easily accommodated in the pyroxene structure. Increasing the Ca concentration should also play a role in changing the size of the Eu anomaly. Following the onset of plagioclase crystallization, Al is depleted in the melt. As Al is a required charge couple in the incorporation of REE^{3+} as per [1]:

$$^{T}Si^{4+} + {}^{M2}R^{2+} \rightarrow {}^{T}Al^{3+} + {}^{M2}REE^{3+},$$

the overall concentration of REE in the late stage pyroxene decreases (Fig.3). XANES analyses provide a means of quantifying the average Eu valence [9], as well as an estimate of f_{O2} at the time of crystallization. During crystallization of early pigeonite to augite, to post-plagioclase-pigeonite, the average Eu valence ranges from ~2.68 to 2.59 to 2.58. Decreasing average Eu valence prior to plagioclase crystallization results from the increasing compatibility of Eu^{2+} in M2 with increasing Ca. XANES and SIMS analyses of plagioclase and pyroxene indicate that plagioclase has a stronger preference for Eu, especially Eu^{2+}. The average Eu valence in plagioclase at both IW and IW+1 is approximately 2.4. The average Eu valence of late stage pyroxene that co-crystallizes with plagioclase is within error of earlier formed augite. This is likely the result of two coeval processes, decreasing Ca in M2 and decreasing Al^{3+}, a necessary charge couple for incorporating REE^{3+} into pyroxene.

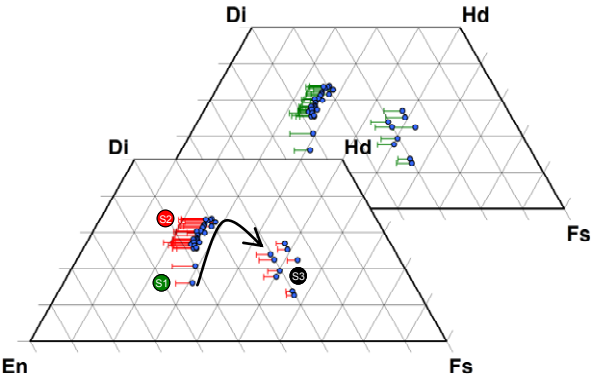

Figure 2. Pyroxene quadrilateral, illustrating the major element chemistry and crystallization trend in QUE 24 (IW+1). Both quads plot the same data points; the quad in the background has scaled error bars (green) illustrating the magnitude of the Ti component, while the quad in the foreground has (red) error bars which illustrate the magnitude of the Al component. Colored SIMS spots as per Fig. 1; the SIMS spots serve to provide context for the analysis, and do not define an actual measured composition.

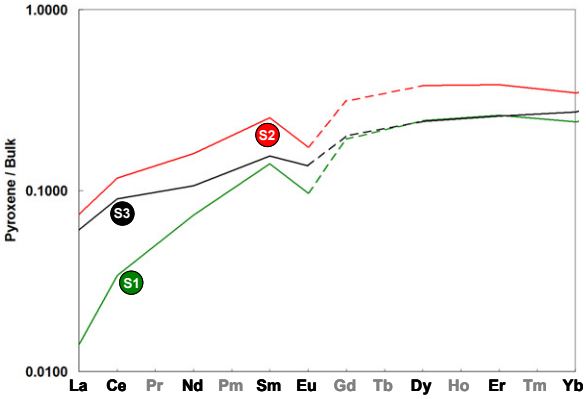

Figure 3. REE plot for SIMS analyses conducted on QUE 24 (IW+1); location of analyses illustrated in Fig.1. S1 and S2 both represent averages of two analyses, while S3 is a single analysis.

Acknowledgements Portions of this work were performed at GeoSoilEnviroCARS (Sector 13), Advanced Photon Source (APS), Argonne National Laboratory. GeoSoilEnviroCARS is supported by the National Science Foundation - Earth Sciences (EAR-0622171) and Department of Energy - Geosciences (DE-FG02-94ER14466). Use of the Advanced Photon Source was supported by the U. S. Department of Energy, Office of Science, Office of Basic Energy Sciences, under Contract No. DE-AC02-06CH11357.

References [1]Shearer et. al. (2006) *AmMin*, **91**, 1565-1573. [2]Philpotts (1970) *EPSL*, **9**, 257-268. [3]Schnetzler and Philpotts (1970) *GeochimCosmochim*, **34**, 333-340. [4]Weill and Drake (1973) *Science*, **180**, 1059-1060. [5]Wadhwa (2001) *Science*, **291**, 1527-1530. [6]Bence and Papike (1972) *Proc3rdLunarScienceConf, 431-469*. [7]Shearer et. al. (1989) *GeochimCosmochim*, **53**, 1041-1054. [8]McKay (1989) *RevInMineral*, **21**, 45-77. [9]Karner et. al. (2010) *AmMin*, **95**, 410-413. [10]Sutton et. al. (2002) *RevInMineral*, **49**, 429-483.